Thermal Transport in Functionalized Graphene

Jeong Yun Kim,[†] Joo-Hyoung Lee,[‡] and Jeffrey C. Grossman[†,*]

[†]Department of Materials Science and Engineering, Massachusetts Institute of Technology, Cambridge, Massachusetts 02139, United States and [‡]School of Materials Science and Engineering, Gwangju Institute of Science and Technology, Gwangju, Republic of Korea

ABSTRACT

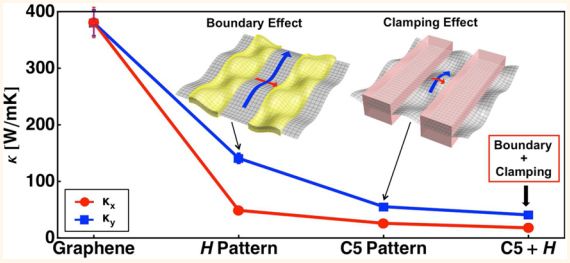

We investigate the effects of two-dimensional (2D) periodic patterns of functional groups on the thermal transport in a graphene monolayer by employing molecular and lattice dynamics simulations. Our calculations show that the use of patterned 2D shapes on graphene reduces the room temperature thermal conductivity, by as much as 40 times lower than that of the pristine monolayer, due to a combination of boundary and clamping effects. Lattice dynamics calculations elucidate the correlation between this large reduction in thermal conductivity and two dynamical properties of the main heat carrying phonon modes: (1) decreased phonon lifetimes by an order of magnitude due to scattering, and (2) direction-dependent group velocities arising from phonon confinement. Taken together, these results suggest that patterned graphene nanoroads provide a method for tuning the thermal conductivity of graphene without the introduction of defects in the lattice, opening an important possibility for thermoelectric applications.

KEYWORDS: thermal conductivity · graphene · chemical functionalization · thermoelectrics · molecular dynamics · lattice dynamics

Graphene has attracted intense attention for both its superior carrier mobility at room temperature and its unique zero-gap band structure, which leads to massless charge carriers.[1,2] In addition to these remarkable electronic properties, there have been recent attempts to use graphene for thermoelectric (TE) applications[3,4] due to its low-dimensional structure and ambipolar nature, controlling the sign of the Seebeck coefficient (S) by changing the gate bias instead of doping. The efficiency of a TE material is determined by its figure of merit, $ZT = S^2\sigma T/\kappa$, where S is the Seebeck coefficient, σ the electrical conductivity, κ the thermal conductivity, and T the temperature. For a pristine graphene monolayer, the TE properties have been studied both theoretically[5−7] and experimentally,[8−10] with reported values for S as high as 100 μV/K, suggesting the potential of graphene as a candidate material for TE applications. However, because of its extremely high κ,[11−13] bare graphene is overall a highly inefficient TE material.[8] Thus, in order to create an efficient ZT material based on graphene, a significant reduction in the thermal conductivity is required.

One way to suppress the thermal conductivity of graphene, or nearly any material, would be to introduce point defects such as interstitials, vacancies, or by alloying. However, if the goal is to explore thermoelectric applications, one must balance reduced thermal conductivity against the need for a large power factor ($S^2\sigma$). Unlike a range of other promising classes of thermoelectric materials that utilize controlled defects (phonon glass) as phonon scattering sites by taking advantage of inherent "electron crystal" properties in the materials, including skutterudites[14] and clathrates,[15] the introduction of *controlled* "rattling structures" into a graphene sheet would pose an enormous synthesis challenge. The use of less controlled defects such as vacancies[16] or substitutional impurities[17] would of course lower the thermal conductivity, but they would also lower the power factor by so much that such an approach is unlikely to be relevant to the case of graphene-based thermoelectrics. Introduction of isotope disorder and isotope patterns would be a method of reducing thermal conductivity of graphene without degrading electron transport; however, because of the relatively marginal thermal conductivity reduction, by only a factor of 2,[18] such approaches also have not led to significant increases in ZT.

Another way to suppress the thermal conductivity of a material is to reduce its dimensionality, for example, by using quantum

* Address correspondence to jcg@mit.edu.

Received for review July 15, 2012 and accepted September 13, 2012.

Published online September 13, 2012
10.1021/nn3031595

wires or superlattices.[19−21] Recent theoretical studies have shown that the thermal conductivity of a graphene nanoribbon (GNR) can be suppressed by several orders of magnitude compared to graphene due to its edge disorder,[3,22−24] which is introduced during fabrication. However, owing to several obstacles to producing GNR-based devices, including the challenge of reliable production of GNRs with controlled width distributions and the manipulation required for assembling as-produced GNRs into devices,[25] it would be advantageous to develop approaches that reduce the thermal conductivity of graphene that do not rely on physical cutting or etching. Toward this end, graphene superlattices made with chemical functionalization are of great interest and have been explored recently due to the possibility of nanostructuring graphene into complex patterns.[25−29] Functionalization also leads to tunable electronic properties by opening the energy gap of graphene, originating from the induced changes in the hybridization of carbon atoms from sp^2 to sp^3.[25,27−29] It is therefore of great interest to further explore the potential of graphene superlattices made with chemical functionalization for TE applications, in particular, the role of such functionalization on thermal transport properties.

Among various kinds of pattern shapes, we focus in this work on 2D periodic line patterns to produce graphene "nanoroads",[25] which are in a sense a mixture of pristine GNRs and GNRs with full functionalization within the same sheet. Such partial functionalization generates patterned sp^3-hybridized carbon regions with well-defined boundaries between the sp^2 (pristine GNR) and sp^3 (functionalized GNR) domains. The key question for such materials regarding TE applications is whether their thermal conductivity can be efficiently suppressed due to the phonon scattering at these boundaries without severely degrading the electronic properties of the pristine monolayer. Here, we study the influence of 2D periodic patterns on the thermal transport of partially functionalized graphene with different functional groups, employing a combination of classical molecular dynamics and lattice dynamics simulations. The thermal conductivity is computed as a function of a range of pattern widths and functional groups (H and hydrocarbon chains). Our calculations demonstrate that the presence of hydrogenated regions leads to thermal conductivities up to 7 times smaller than that of pristine graphene in the direction perpendicular to the pattern boundary, due to a combination of scattering at the interface and phonon confinement effects. Such a reduction alone would not be sufficient to make graphene-based TE practical. However, we find that an additional reduction by a factor of more than 20 is obtained in patterned graphene with hydrocarbon chains, due to a "clamping" effect of the chains arising from their steric repulsion, as well as scattering between sp^2 and sp^3 carbon. We show that combining both types of functional groups further reduces the thermal conductivity in both perpendicular and parallel directions to the pattern boundary (by as much as 40× in our calculations for the perpendicular direction), implying that chemical functionalization could be an efficient route to engineering the thermal transport in graphene monolayers.

RESULTS AND DISCUSSION

In our simulations, patterned graphene nanoroads are formed *via* partial functionalization of graphene sheets with the armchair-type of interface, which has a geometry that remains completely flat upon structural relaxation (see Figure 1a).[25] Graphene is functionalized with H atoms and hydrocarbon chains (pentane C_5H_{12}, referred to as C5) on both sides of the sheet in an

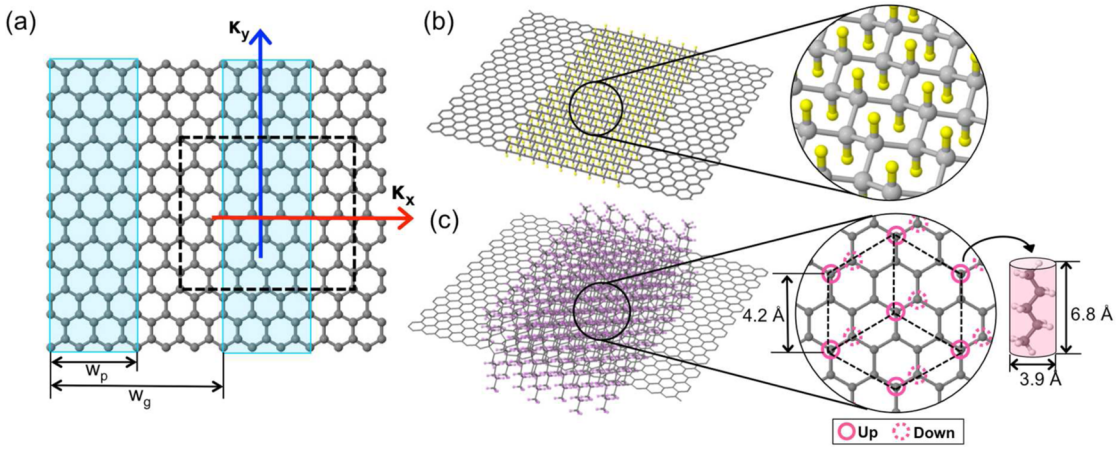

Figure 1. (a) Schematic representation of a patterned graphene sample with an armchair-type boundary along with structural variables used in the calculations. Blue shaded area indicates the patterned region, and the black dotted square represents the MD simulation unit cell. (b) Unit cell of H-functionalized graphene with graphane structure (inset). (c) C5-functionalized graphene. The inset shows the C sites of graphene where C5 chains are attached, arranged in a two-dimensional hexagonal close-packed lattice, as well as the structure of C5 (pentane: C_5H_{12}).

alternating manner.[30] While H atoms can be attached to each C site of graphene to make graphane (see Figure 1b),[29] it is not possible to functionalize graphene with C5 chains in the same fashion as for H atoms due to the steric repulsion between the chains (see Figure 1c).[31] Thus, we model the densest packing of C5 chains on graphene possible, given the possible bonding configurations available in the graphene lattice, namely, a close-packed array of C5 chains separated by 4.2 Å, as shown in Figure 1c.

Molecular Dynamics Simulations. Molecular dynamics (MD) simulations are employed within the LAMMPS package[32] to compute thermal conductivities for all of the systems considered in this work. We first compute the thermal conductivity of approximately square graphene sheets ranging in size from 20 to 500 Å (corresponding to 200−92 000 atoms in the simulation cell) and find that κ converges to the value of 350 W/mK for sizes larger than 50 Å (see Supporting Information), in good agreement with previous simulation results using the REBO potential.[33−35] On the basis of these convergence tests, we choose the size of graphene superlattices to be 50 Å for all subsequent simulations. We define the pattern coverage as W_p/W_g, where W_p and W_g are the functionalized and pristine graphene widths, respectively. Figure 2 shows our computed values of κ_x and κ_y (perpendicular and parallel to the pattern boundary, respectively) for hydrogen-functionalized graphene as a function of pattern coverage. In the case of H functionalization (HG), κ_x shows a more than 7-fold reduction from that of bare graphene over a wide range of coverage except for the fully hydrogenated graphane, which is lower than that of graphene due to the full conversion from sp^2 to sp^3 bonding,[36] although substantially higher than intermediate coverage values since there are no longer boundary scattering effects. For thermal transport parallel to the boundary, one might expect a simple rule of mixtures to apply, although our computed values for κ_y are 2× lower than what would be expected and even lower than κ of graphane, slightly decreasing with

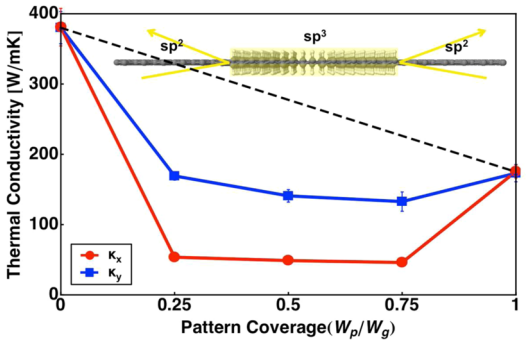

Figure 2. Thermal conductivities of HG samples both perpendicular (red) and parallel (blue) to the pattern as a function of H pattern coverage. Black dotted line corresponds to the predicted κ_y from the rule of mixtures.

the pattern coverage. This reduction is due to the presence of a well-defined boundary between pristine graphene (sp^2) and graphane (sp^3), where the acoustic mismatch at the interface gives rise to incoherent scattering, particularly for high-frequency modes,[37] and scattered phonons reduce κ_y below the predictions from the rule of mixtures. However, for partial coverage values, κ_x is essentially constant and substantially further reduced compared to κ_y. In addition to the effects of boundary scattering, the acoustic mismatch between pristine graphene and graphane also gives rise to a phonon confinement effect, which partially localizes low-frequency phonon modes[37] within the graphene or graphane domains, further reducing the thermal conductivity in the perpendicular direction by a factor of 3 compared to the parallel direction. This phenomenon has been observed in previous studies of in-plane thermal transport in superlattices, where it has been shown that phonon confinement arises from the acoustic mismatch at the boundary resulting in a modified dispersion with lower group velocity.[38,39] Interestingly, in contrast to these other materials systems, in the case of hydrogenated graphene, it is the structural difference (*i.e.*, sp^2 *vs* sp^3) that causes the acoustic mismatch, not a large mass difference between the two domains. Note that for partial coverage values κ_x is nearly independent of the pattern coverage due to the fact that the boundary region per unit area is a constant (0.4/nm), which leads to near-constant boundary scattering and phonon confinement effects. Therefore, in HG cases, the large κ reduction in both directions mainly arises from the presence of the sharp boundary between graphene and graphane domains.

When graphene is functionalized with patterns of C5 chains (C5G), both κ_x and κ_y are further reduced from those of HG (see Figure 3a), with the lowest κ value 22 times smaller than that of pristine graphene at full coverage. It is interesting to note that the behavior of κ with pattern coverage is considerably different compared to the HG case. This can be explained from the different type of functionalization that results in unfunctionalized carbon atoms in the patterned region around the C5 chains due to the steric repulsion between chains (see Figure 1c). This functionalization can generate two thermal conductivity reduction mechanisms, each of which can lead to a strong decrease: a clamping effect and scattering between sp^2 and sp^3 carbon in the patterned region. The C5 chains give rise to cuboid-shaped regions on both sides of graphene, which effectively clamp the graphene sheet from both sides due to a combination of the heavy mass (71 times larger than H) and large steric volume of the C5 chains. In order to investigate this clamping effect, we calculate the atomic fluctuation of carbon atoms along the *z* direction in each system. As shown in Figure 3b, the fluctuation in the fully functionalized C5G system shows damped behavior compared to the bare

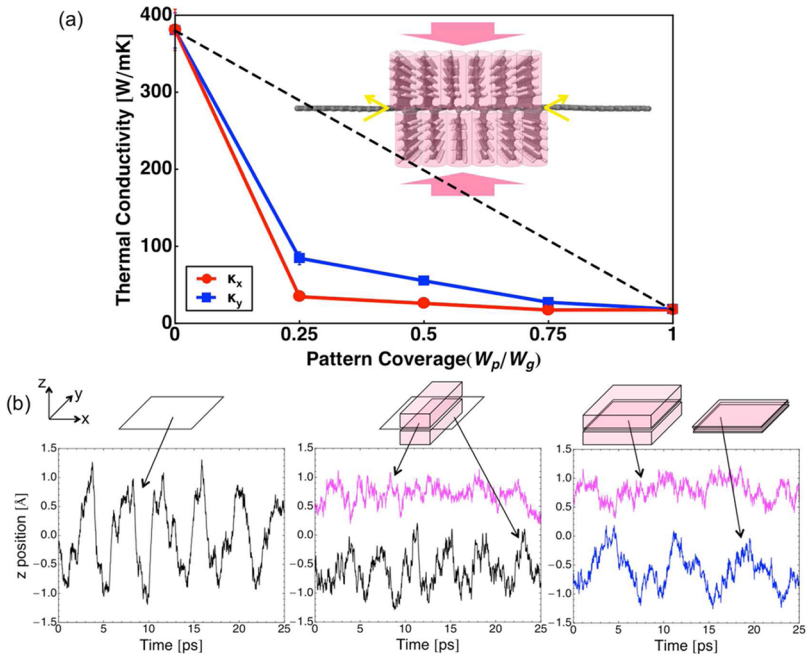

Figure 3. (a) Thermal conductivities of C5G samples as a function of C5 pattern coverage. Black dotted line is for the predicted κ_y from the rule of mixtures; (b) *z* position *vs* time of carbon atoms in pristine graphene (left), partially functionalized C5G (middle), and fully functionalized C5G (right) with schematic figures of our graphene samples (black arrows). The black (pink) solid lines indicate the fluctuation of unpatterned (patterned) regions. The blue line in the plot on the right is for the graphene functionalized with "fake" (heavy) hydrogen atoms.

graphene system, and this damped phonon wave indicates considerably suppressed out-of-plane (ZA) phonon modes in graphene; it has been shown theoretically that as much as 77% of the total thermal conductivity in graphene at room temperature is due to the ZA mode.[8,40] The importance of the ZA mode is supported by the fact that the clamping effect accounts for roughly 50% of the reduction of κ for the fully functionalized C5G system (see Supporting Information). Within this clamping effect, we can separate the two contributions—steric and mass—by carrying out simulations with "fake" hydrogen atoms that have the same mass as a C5 chain but do not have any steric effects. Our results show that roughly 70% of the clamping effect arises from the heavier mass of C5 chains, and 30% arises from steric volume of the C5 chains. It is also interesting to note that out-of-plane fluctuations in graphene with fake hydrogen atoms (mass effect) are larger than those in the C5G system (which contains both mass + steric effects), although smaller than the fluctuations in bare graphene, as expected given our results for κ. In addition to the clamping effect, the other 50% reduction in thermal conductivity arises from the scattering between sp^2 and sp^3 carbon (see Supporting Information). Note that there is no sharp boundary between these regions in the C5G case, although unlike in the HG case, the scattering between sp^2 and sp^3 carbon occurs both between the patterned and unpatterned regions as well as within the patterned region itself.

For partially functionalized C5G samples, κ_y is approximately 3.5 times lower than what would be expected from a simple rule of mixtures, due to spatial confinement of the phonons in the unpatterned region (see Figure 4), which arises from the clamped boundary between the patterned and unpatterned regions. This can be explained by the damped fluctuation in unpatterned regions compared to that in the pristine graphene sample (see Figure 3b). With increasing C5 pattern coverage, κ_y reduces further due to the increased spatial confinement with decreased unpatterned region width, and this behavior is in good agreement with previous work on the effects of quantum wells, where thermal conductivities significantly decrease with well width due to spatial confinement of acoustic phonons.[41] In the C5G system, the anisotropy of thermal conductivity is still present ($\kappa_x/\kappa_y \sim 1/2$), although substantially weaker than HG cases. Damped atomic fluctuations in the clamped region produce a partially damped wave as shown schematically in Figure 4 (lower right) along the perpendicular direction to the pattern in partially functionalized C5G samples. Due to this damped wave propagation, thermal transport along the perpendicular direction is suppressed by a factor of 2 compared to the parallel direction. Thus, in contrast to the case of HG, for C5G, suppressed thermal transport is due to a combination of scattering and clamping effects of the C5 pattern, and these effects can further suppress thermal conductivity not only perpendicular but also parallel to the boundary.

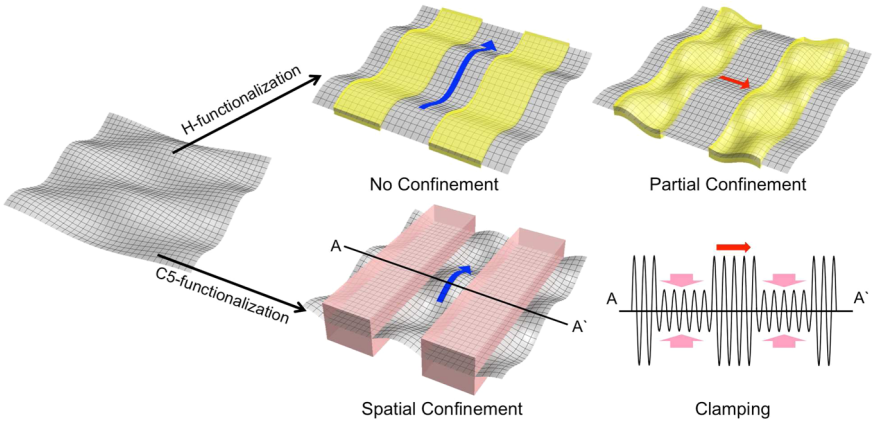

Figure 4. Schematic of phonon confinement effects in graphene with the two different functionalizations considered in this work: hydrogen (top) and C5 chain (bottom). H functionalization induces partial confinement of phonon modes in both graphene and graphane domains and suppresses thermal transport perpendicular to the boundary in HG samples. Modes with no confinement can propagate in all domains and have no effect on thermal transport. C5 functionalization induces spatial confinement due to a clamping effect in the functionalized domain, which suppresses thermal transport parallel to the pattern. The lower right image indicates phonon waves along the AA′ line in the C5G sample; waves in the patterned region (pink arrows) are damped due to the clamping effect, and this partially damped wave suppresses thermal transport in the perpendicular direction. Blue (red) arrows indicate heat transport along parallel (perpendicular) direction to the pattern boundary.

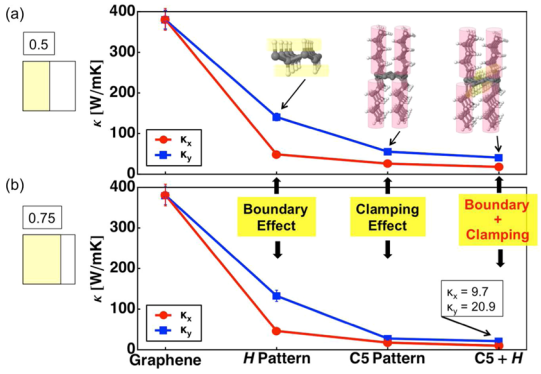

Figure 5. Thermal conductivities of patterned graphene as a function of functional groups are shown for (a) 0.5 and (b) 0.75 pattern coverage. Each functional group introduces different thermal conductivity reduction effects as indicated.

By combining HG and C5G functionalization into the same sample, a further reduction in thermal conductivity can be achieved. In this case, all carbon atoms in the patterned region of graphene can have sp^3 bonding, and a well-defined boundary between graphene (sp^2) and graphane (sp^3) is formed. Combining both boundary and clamping effects in this manner is found to reduce κ to 9.7 W/mK, which is 40 times smaller than that of pristine graphene within our calculations (see Figure 5).

Lattice Dynamics Calculations. In order to analyze the properties of the main heat carriers in functionalized graphene and understand how they differ from those of pristine graphene, we carried out a series of lattice dynamics calculations. We compute the group velocities and lifetimes of each phonon mode in order to quantify their contributions to the thermal conductivity.

In pristine graphene, our calculations show that there are five main heat carrying phonon modes (see Figure 6), each of whose contribution to κ is larger than 4% of the total thermal conductivity. As expected, the low-frequency phonon modes account for most of the thermal conductivity. For the case of hydrogen functionalization, we examine a system with 0.5 pattern coverage. Our calculations show that, due to the presence of a well-defined boundary, the lifetimes of phonon modes below 20 THz are greatly decreased with respect to those in pristine graphene, which makes a large contribution to the decrease of thermal conductivity in the direction both perpendicular and parallel to the pattern, as found in our MD simulations.

It is also observed that the group velocities (v_g) of the main heat carrying modes in HG samples are different in the two directions: v_g in the direction perpendicular to the pattern ($v_{g,x}$) is much lower than in the parallel direction ($v_{g,y}$). As mentioned, this is because of an acoustic mismatch at the boundary, which leads to a modification of the phonon dispersion and group velocities. For instance, in phonon modes 2, 4, and 5, whose total contributions to κ_y are roughly 20%, we find that $v_{g,x}$ is more than 20× smaller than $v_{g,y}$, resulting in a 400× smaller κ_x than κ_y. The fact that these phonon modes cannot carry heat in the direction perpendicular to the pattern while carrying heat in the parallel direction is due to partial confinement in either domain. Note that the shape of these modes (see Figure 6) is nearly consistent with the previous expectation for partial confinement in HG samples (see Figure 4), where phonon modes in either domain exist separately. However, phonon modes 1, 3, and 6, which are consistent with waves with no confinement, contribute to heat conduction in both directions. From lattice dynamics calculations, we find that about 20% of phonon modes in κ_y in our HG sample is frozen out in

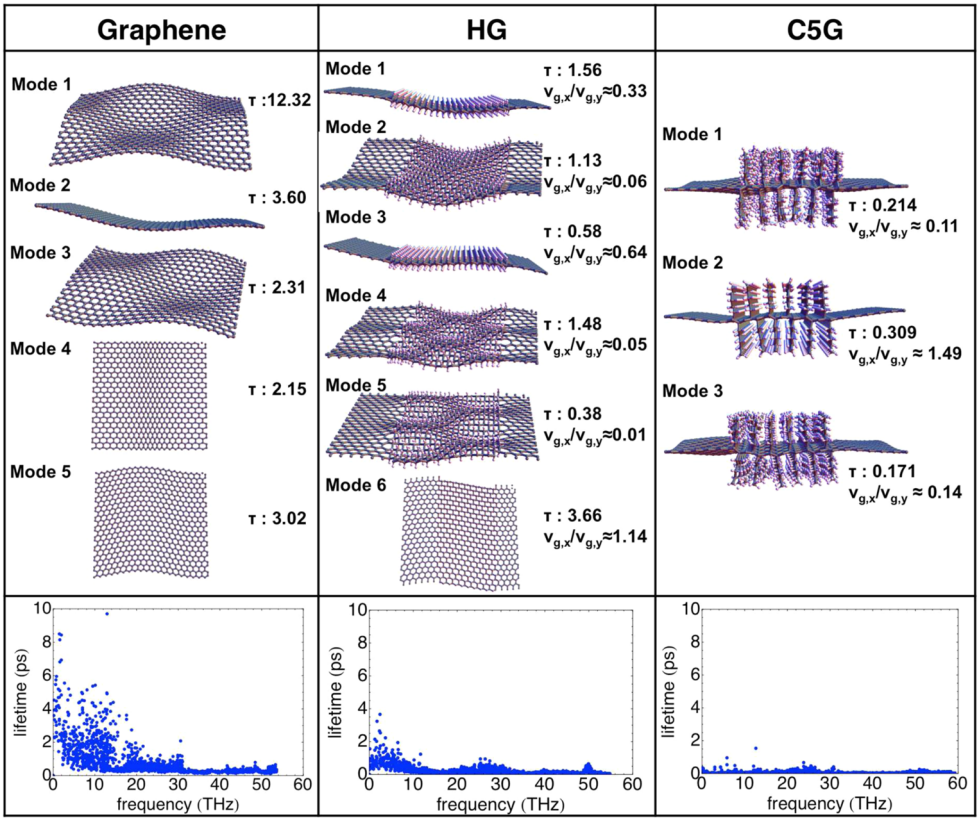

Figure 6. Main heat carrying phonon modes, whose κ contribution is larger than 4% of total κ, for pristine graphene and HG and C5G samples with 50% coverage. Corresponding lifetimes and group velocity ratios for these particular modes are listed, and lifetimes for all frequencies in each sample are also shown (bottom graphs).

the perpendicular direction due to partial phonon confinement, and the other 80% contributes to perpendicular thermal transport in HG samples with reduced group velocities. This thermal transport phenomenon leads to the thermal conductivity difference in directions, consistent with the fact that κ_x/κ_y is 0.346 in this HG sample.

For the C5G case, our calculations show a further reduction of the phonon lifetimes, especially for the low-frequency modes, which is consistent with the large decrease of both κ_x and κ_y. As discussed above, the large reduction in lifetime can be understood by scattering between sp^2 and sp^3 carbon induced from the particular kind of functionalization pattern of C5 chains on graphene.

In C5G samples, $v_{g,x}/v_{g,y}$ values can be larger than 1 (*e.g.*, mode 2) due to the spatial phonon confinement in unpatterned graphene regions, resulting in a strong modification of the phonon dispersion and reduction of group velocities in the parallel direction to the pattern.[41] Moreover, partially damped waves in C5G samples further reduce group velocities in the perpendicular direction, as can be seen from modes 1 and 3. Although all of the main heat carrying phonon modes of the C5G sample contribute to heat conduction in both directions with different contributions, thermal conduction in the perpendicular direction is roughly 2× lower than in the parallel direction, consistent with the larger value of κ_x/κ_y, 0.469, than that of HG samples.

CONCLUSIONS

Chemical functionalization plays a significant role in the thermal transport of 2D materials since all atoms in the system can be functionalized, and phonon modes can be widely modified, suggesting many possibilities for tuning thermal transport, in contrast to the case of 3D where only surface atoms can be functionalized, leading to a minor influence on thermal transport. In this work, we performed molecular and lattice dynamics calculations to study the effect of chemical functionalization on thermal transport of graphene monolayers. Our simulations demonstrate that the presence of 2D periodic patterns on a graphene sheet suppresses thermal conductivity due to two main effects: (1) boundary effects induced from the sharp interface between sp^2 and sp^3 carbon domains and (2) clamping effects induced from both the additional mass as well as steric packing of hydrocarbon chains. Introducing boundaries in materials by nanostructuring has been widely used to reduce thermal conductivity.[19−21] In the present work, we propose an approach for reducing the thermal conductivity in graphene based on steric hindrance, which could be applied to other fluctuating materials, such as 1D carbon nanotubes and

2D boron nitride sheets. By combining steric hindrance with boundary scattering, we predict a reduction of the thermal conductivity by as much as a factor of 40 compared to pristine graphene. Our results suggest that chemical functionalization could broadly tailor thermal transport in a low-dimensional system with different chemistries that change mass, charge, and shape of functional groups as well as functionalized configuration. For example, using planar molecules such as benzene or azobenzene, which would induce more closely packed functionalization providing a stronger clamping effect, the thermal conductivity reduction could be even further enhanced. Further, the presence of a second layer of graphene together with chemical functionalization can have a similar effect; our calculations on C5+H samples with half-coverage show a reduction from 18 W/mK in the single-layer case to 11 W/mK for a bilayer. These results suggest that the tunable thermal conductivity of functionalized graphene could lead to its use as an efficient thermoelectric material.[24,42,43]

METHODS

Molecular Dynamics Simulations. The thermal conductivity is computed from the fluctuations of the heat current, using the Einstein relation.[44,45]

$$\kappa_\alpha = \frac{1}{k_B V T^2} \lim_{t\to\infty} \frac{1}{2t} \langle [R_\alpha(t) - R_\alpha(0)]^2 \rangle$$

where k_B is the Boltzmann constant, V the system volume, and T the temperature. $\langle [R_\alpha(t) - R_\alpha(0)]^2 \rangle$ is the mean square displacement of the integrated microscopic heat flux along the α direction, given by $R_\alpha = \sum_i \varepsilon_{i\alpha} r_{i\alpha}$, where ε_i is the energy of atom i at position r_i. The volume is calculated as the product of the unit cell planar area times the interplanar distance (3.35 Å). To describe the covalent bonding interactions in the carbon and hydrocarbon systems, we used the second-generation reactive empirical bond order (REBO)[46] potential, which has been successfully used in many carbon-based systems, such as carbon nanotubes and graphene, for thermal transport studies.[33−35] All simulations are carried out at 300 K with a time step of 0.2 fs. To obtain converged results, 10 separate simulations are averaged for each system, each with different initial conditions. In each run, after a 100 ps equilibration period, the microscopic heat flux in the directions perpendicular and parallel to the functionalization pattern are recorded for 10^7 MD steps (2 ns) in order to obtain a converged thermal conductivity value.

Lattice Dynamics Calculations. The group velocities can be determined from the phonon dispersion around the Γ point of the Brillouin zone in a large supercell. We consider $0 \le |\vec{q}| \le 0.002$ Å^{-1}, where $\vec{q}$ is a phonon wavevector and is spaced by 0.0001 Å^{-1}. Approximating the dispersion curves by a quadratic function, the group velocity is obtained from the slope at $\vec{q} = 0.002$ Å^{-1}. The phonon lifetime (τ_i) is computed from the integral of the normalized autocorrelation function of the kinetic energy fluctuation of the eigenmodes[47]

$$\tau_i = \int_0^\infty \frac{\langle \delta E_{i,k}(\vec{q},t)\delta E_{i,k}(\vec{q},0)\rangle}{\langle \delta E_{i,k}(\vec{q},0)\delta E_{i,k}(\vec{q},0)\rangle} dt$$

where

$$E_{i,k}(\vec{q},t) = \frac{A_i'^* A_i'}{2}$$

$$A_i(\vec{q},t) = \sum_j \sqrt{M_j} e^{(-i\vec{q}\cdot\vec{r}_{j,0})} \varepsilon_i^*(\vec{q}) \cdot u_j(t)$$

By projecting the atomic trajectories generated by MD simulations on the normal mode coordinates, we obtain a time history of the normal mode amplitudes $A_i(\vec{q},t)$, which gives the mode kinetic energy, $E_{i,k}$. Here, M_j is the mass of j-th atom, $r_{j,0}$ the equilibrium position, and u_j the relative displacement from its equilibrium position in our MD trajectories; ε_i is an eigenvector obtained from lattice dynamics calculation. The contribution to κ from i-th phonon mode (κ_i) is expressed in terms of group velocities v_i and lifetimes τ_i, using the single mode relaxation time approximation of the Boltzmann transport equation[48]

$$\kappa_i(\vec{q}) = C_i(\vec{q}) v_i^2(\vec{q}) \tau_i(\vec{q})$$

Here C_i is the specific heat per unit volume of i-th phonon mode from the Bose-Einstein statistics

$$C_i(\vec{q}) = \frac{1}{V} k_B x^2 \frac{e^x}{(e^x - 1)^2}$$

where $x = \hbar\omega_i(\vec{q})/k_B T$ and $\omega_i(\vec{q})$ is the phonon frequency.

Conflict of Interest: The authors declare no competing financial interest.

Acknowledgment. The authors thank P. A. Greaney for useful discussions of lattice dynamics calculations. This work was funded by the Defense Threat Reduction Agency—Joint Science and Technology Office for Chemical and Biological Defense (Grant HDTRA1-09-1-0006). Calculations were performed using NERSC computing resources.

Supporting Information Available: Additional simulation details. This material is available free of charge *via* the Internet at http://pubs.acs.org.

REFERENCES AND NOTES

1. Geim, A. K.; Novoselov, K. S. The Rise of Graphene. *Nat. Mater.* **2007**, *6*, 183–191.
2. Charlier, J. C.; Eklund, P. C.; Zhu, J.; Ferrari, A. C. Electron and Phonon Properties of Graphene: Their Relationship with Carbon Nanotubes. In *Carbon Nanotubes*; Jorio, A., Dresselhaus, G., Dresselhaus, M. S., Eds.; Topics in Applied Physics 111; Springer: New York, 2008; pp 673−709.
3. Sevincli, H.; Cuniberti, G. Enhanced Thermoelectric Figure of Merit in Edge-Disordered Zigzag Graphene Nanoribbons. *Phys. Rev. B* **2010**, *81*, 113401.
4. Kageshima, H.; Hibino, H.; Nagase, M.; Sekine, Y.; Yamaguchi, H. Theoretical Study on Magnetoelectric and Thermoelectric Properties for Graphene Devices. *Jpn. J. Appl. Phys.* **2011**, *50*, 070115.
5. Bao, W. S.; Liu, S. Y.; Lei, X. L. Thermoelectric Power in Graphene. *J. Phys.: Condens. Matter* **2010**, *22*, 315502.
6. Dragoman, D.; Dragoman, M. Giant Thermoelectric Effect in Graphene. *Appl. Phys. Lett.* **2007**, *91*, 203116.
7. Hwang, E. H.; Rossi, E.; Das Sarma, S. Theory of Thermopower in Two-Dimensional Graphene. *Phys. Rev. B* **2009**, *80*, 235415.
8. Seol, J. H.; Jo, I.; Moore, A. L.; Lindsay, L.; Aitken, Z. H.; Pettes, M. T.; Li, X. S.; Yao, Z.; Huang, R.; Broido, D.; *et al.* Two-Dimensional Phonon Transport in Supported Graphene. *Science* **2010**, *328*, 213–216.
9. Zuev, Y. M.; Chang, W.; Kim, P. Thermoelectric and Magnetothermoelectric Transport Measurements of Graphene. *Phys. Rev. Lett.* **2009**, *102*, 096807.
10. Wei, P.; Bao, W. Z.; Pu, Y.; Lau, C. N.; Shi, J. Anomalous Thermoelectric Transport of Dirac Particles in Graphene. *Phys. Rev. Lett.* **2009**, *102*, 166808.

11. Balandin, A. A.; Ghosh, S.; Bao, W. Z.; Calizo, I.; Teweldebrhan, D.; Miao, F.; Lau, C. N. Superior Thermal Conductivity of Single-Layer Graphene. *Nano Lett.* **2008**, *8*, 902–907.
12. Ghosh, S.; Calizo, I.; Teweldebrhan, D.; Pokatilov, E. P.; Nika, D. L.; Balandin, A. A.; Bao, W.; Miao, F.; Lau, C. N. Extremely High Thermal Conductivity of Graphene: Prospects for Thermal Management Applications in Nanoelectronic Circuits. *Appl. Phys. Lett.* **2008**, *92*, 151911.
13. Nika, D. L.; Pokatilov, E. P.; Askerov, A. S.; Balandin, A. A. Phonon Thermal Conduction in Graphene: Role of Umklapp and Edge Roughness Scattering. *Phys. Rev. B* **2009**, *79*, 155413.
14. Uher, C. Skutterudites: Prospective Novel Thermoelectrics. *Semicond. Semimetals* **2001**, *69*, 139–253.
15. Nolas, G. S.; Poon, J.; Kanatzidis, M. Recent Developments in Bulk Thermoelectric Materials. *MRS Bull.* **2006**, *31*, 199–205.
16. Zhang, H. J.; Lee, G.; Cho, K. Thermal Transport in Graphene and Effects of Vacancy Defects. *Phys. Rev. B* **2011**, *84*, 115460.
17. Jiang, J. W.; Wang, B. S.; Wang, J. S. First Principle Study of the Thermal Conductance in Graphene Nanoribbon with Vacancy and Substitutional Silicon Defects. *Appl. Phys. Lett.* **2011**, 98.
18. Chen, S. S.; Wu, Q. Z.; Mishra, C.; Kang, J. Y.; Zhang, H. J.; Cho, K. J.; Cai, W. W.; Balandin, A. A.; Ruoff, R. S. Thermal Conductivity of Isotopically Modified Graphene. *Nat. Mater.* **2012**, *11*, 203–207.
19. Li, D. Y.; Wu, Y. Y.; Kim, P.; Shi, L.; Yang, P. D.; Majumdar, A. Thermal Conductivity of Individual Silicon Nanowires. *Appl. Phys. Lett.* **2003**, *83*, 2934–2936.
20. Donadio, D.; Galli, G. Atomistic Simulations of Heat Transport in Silicon Nanowires. *Phys. Rev. Lett.* **2009**, *102*, 195901.
21. Lee, S. M.; Cahill, D. G.; Venkatasubramanian, R. Thermal Conductivity of Si-Ge Superlattices. *Appl. Phys. Lett.* **1997**, *70*, 2957–2959.
22. Savin, A. V.; Kivshar, Y. S.; Hu, B. Suppression of Thermal Conductivity in Graphene Nanoribbons with Rough Edges. *Phys. Rev. B* **2010**, *82*, 195422.
23. Hu, J. N.; Ruan, X. L.; Chen, Y. P. Thermal Conductivity and Thermal Rectification in Graphene Nanoribbons: A Molecular Dynamics Study. *Nano Lett.* **2009**, *9*, 2730–2735.
24. Nika, D. L.; Balandin, A. A. Two-Dimensional Phonon Transport in Graphene. *J. Phys.: Condens. Matter* **2012**, 24.
25. Singh, A. K.; Yakobson, B. I. Electronics and Magnetism of Patterned Graphene Nanoroads. *Nano Lett.* **2009**, *9*, 1540–1543.
26. Boukhvalov, D. W.; Katsnelson, M. I. Chemical Functionalization of Graphene. *J. Phys.: Condens. Matter* **2009**, *21*, 344205.
27. Sessi, P.; Guest, J. R.; Bode, M.; Guisinger, N. P. Patterning Graphene at the Nanometer Scale *via* Hydrogen Desorption. *Nano Lett.* **2009**, *9*, 4343–4347.
28. Balog, R.; Jorgensen, B.; Nilsson, L.; Andersen, M.; Rienks, E.; Bianchi, M.; Fanetti, M.; Laegsgaard, E.; Baraldi, A.; Lizzit, S.; *et al.* Bandgap Opening in Graphene Induced by Patterned Hydrogen Adsorption. *Nat. Mater.* **2010**, *9*, 315–319.
29. Elias, D. C.; Nair, R. R.; Mohiuddin, T. M. G.; Morozov, S. V.; Blake, P.; Halsall, M. P.; Ferrari, A. C.; Boukhvalov, D. W.; Katsnelson, M. I.; Geim, A. K.; *et al.* Control of Graphene's Properties by Reversible Hydrogenation: Evidence for Graphane. *Science* **2009**, *323*, 610–613.
30. Sofo, J. O.; Chaudhari, A. S.; Barber, G. D. Graphane: A Two-Dimensional Hydrocarbon. *Phys. Rev. B* **2007**, *75*, 153401.
31. Torrent-Sucarrat, M.; Liu, S. B.; De Proft, F. Steric Effect: Partitioning in Atomic and Functional Group Contributions. *J. Phys. Chem. A* **2009**, *113*, 3698–3702.
32. Plimpton, S. Fast Parallel Algorithms for Short-Range Molecular-Dynamics. *J. Comput. Phys.* **1995**, *117*, 1–19.
33. Ong, Z. Y.; Pop, E. Effect of Substrate Modes on Thermal Transport in Supported Graphene. *Phys. Rev. B* **2011**, *84*, 075471.
34. Zhang, H. J.; Lee, G.; Fonseca, A. F.; Borders, T. L.; Cho, K. Isotope Effect on the Thermal Conductivity of Graphene. *J. Nanomater.* **2010**, 537657.
35. Chien, S. K.; Yang, Y. T.; Chen, C. K. Influence of Hydrogen Functionalization on Thermal Conductivity of Graphene: Nonequilibrium Molecular Dynamics Simulations. *Appl. Phys. Lett.* **2011**, *98*, 033107.
36. Pei, Q. X.; Sha, Z. D.; Zhang, Y. W. A Theoretical Analysis of the Thermal Conductivity of Hydrogenated Graphene. *Carbon* **2011**, *49*, 4752–4759.
37. Zhao, H.; Freund, J. B. Phonon Scattering at a Rough Interface between Two Fcc Lattices. *J. Appl. Phys.* **2009**, 105.
38. Chen, G. Phonon Wave Heat Conduction in Thin Films and Superlattices. *J. Heat Transfer* **1999**, *121*, 945–953.
39. Hyldgaard, P.; Mahan, G. D. Phonon Superlattice Transport. *Phys. Rev. B* **1997**, *56*, 10754–10757.
40. Lindsay, L.; Broido, D. A.; Mingo, N. Flexural Phonons and Thermal Transport in Graphene. *Phys. Rev. B* **2010**, *82*, 115427.
41. Balandin, A.; Wang, K. L. Effect of Phonon Confinement on the Thermoelectric Figure of Merit of Quantum Wells. *J. Appl. Phys.* **1998**, *84*, 6149–6153.
42. Balandin, A. A. Thermal Properties of Graphene and Nanostructured Carbon Materials. *Nat. Mater.* **2011**, *10*, 569–581.
43. Balandin, A. A.; Nika, D. L. Phononics in Low-Dimensional Materials. *Mater. Today* **2012**, *15*, 266–275.
44. Weitz, D. A.; Pine, D. J.; Pusey, P. N.; Tough, R. J. A. Nondiffusive Brownian-Motion Studied by Diffusing-Wave Spectroscopy. *Phys. Rev. Lett.* **1989**, *63*, 1747–1750.
45. Viscardy, S.; Servantie, J.; Gaspard, P. Transport and Helfand Moments in the Lennard-Jones Fluid. II. Thermal Conductivity. *J. Chem. Phys.* **2007**, *126*, 184513.
46. Brenner, D. W.; Shenderova, O. A.; Harrison, J. A.; Stuart, S. J.; Ni, B.; Sinnott, S. B. A Second-Generation Reactive Empirical Bond Order (REBO) Potential Energy Expression for Hydrocarbons. *J. Phys.: Condens. Matter* **2002**, *14*, 783–802.
47. Ladd, A. J. C.; Moran, B.; Hoover, W. G. Lattice Thermal-Conductivity - A Comparison of Molecular-Dynamics and Anharmonic Lattice-Dynamics. *Phys. Rev. B* **1986**, *34*, 5058–5064.
48. McGaughey, A. J. H.; Kaviany, M. Quantitative Validation of the Boltzmann Transport Equation Phonon Thermal Conductivity Model under the Single-Mode Relaxation Time Approximation. *Phys. Rev. B* **2004**, *69*, 094303.